Progress In Electromagnetics Research M, Vol. 39, 41–52, 2014

Improvement of the Coupling Factor of Litz-Wire Coil Pair with Ferrite Substrate for Transcutaneous Energy Transfer System

Le Ke*, Guozheng Yan, Sheng Yan, Zhiwu Wang, and Dasheng Liu

Abstract—This paper presents an optimized design of Litz-wire coil pair with ferrite substrates based on a set of analytical expressions and a 2-D finite-element analysis (FEA) in a way that the coupling coefficient is maximized. An investigation is made on key structure parameters of coils (e.g., structure of Litz-wire, number of turns, and number of layers) to determine their influence on self-inductance and mutual inductance respectively. The influence of ferrite substrate (e.g., relative permeability and thickness) is also considered. Different types of fabricated coils are used to verify all analytical expressions and optimization methods, and it is found that the theoretical predictions and simulations are in agreement with the measured results.

1. INTRODUCTION

In order to reduce the risk of postoperative infection and patient discomfort, transcutaneous energy transfer system (TETS) is widely applied to wireless powering of implantable biomedical devices, such as left ventricular assist devices (LVAD) [1], artificial anal sphincters [2, 3], artificial retinas [4], and wireless neurostimulators [5]. The performance of TETS largely depends on the high power transfer efficiency (PTE), which is imperative to minimize the size of the external drive source, heating of the tissue, and interference with other devices. The most effective way to improve the PTE is to increase the coupling coefficient between the two coils. Generally speaking, two kinds of planar coils have been designed and documented in several researches. The first type is the printed spiral coils (PSC), which may be further broken down into either rigid or flexible types, and such a type is applicable to those cases with requirements of low power, high frequency and strict size constrain (intraocular or intracranial space) [6, 7]. One example of a flexible PSC fabricated with a liquid metal alloy encased in a biocompatible elastomeric substrate is the retinal prosthesis system [8]. This system utilizes an inductive transfer link to wirelessly deliver 100 mW of power to the flexible micro-coil implanted inside the eye with 21% PTE (4 MHz) at a 12 mm separation. Filament wire coil, such as Litz-wire coil, is another planar structure that comprises multiple individually insulated strands. This kind of coil is suitable for applications with requirements of significant power but less size constrains. As described in [1], TETS with Litz-wire coils can transmit electric energy 20 W with a tissue thickness of 5 mm$\sim$15 mm at an efficiency of over 85%. In addition, ferrite components have been successfully used to constrain flux to desired paths in order to improve coupling between coils and consequently prevent excessive loss of surrounding materials caused by magnetic field leakage [9, 10]. However, to the best of our knowledge, optimized design of Litz-wire coil pair with ferrite substrate in a way that the coupling coefficient is maximized with respect to the structure and geometry of planar Litz-wire coils as well as the influence of the magnetic substrate via modeling analysis remains to be further addressed in the published literature.

This research focuses on investigating the coupling coefficient between two Litz-wire coils with ferrite substrates suitable for a artificial anal sphincter system (AASS) for treating severe fecal

Received 6 August 2014, Accepted 15 August 2014, Scheduled 30 September 2014

* Corresponding author: Lei Ke (suda_kelei@163.com).

The authors are with the Institute of Medical Precision Engineering and Intelligent System, Department of Instrument Science and Engineering, Shanghai Jiaotong University, Shanghai, P. R. China.

incontinence (FI) [11], and using appropriate analytical, simulation and experimental data to optimize the coil design. Some compact models for predicting self inductance and mutual inductance are presented. The proposed model calculates the prediction based on winding characteristics, substrate properties, and geometric parameters of the planar coils as well as relative placement of the coils in the TETS. On such foundation, we devised an appropriate coil design method starting with a set of realistic constrains and ending with the optimal coil pair geometries. A simulation approach with finite element analysis (FEA) was used in this work; therefore, experimental results of some prototypes are included to confirm the validity of the theory and optimization method.

2. COUPLING ANALYSIS

2.1. System Overview

Figure 1 shows a schematic circuit representation of a TETS applied in AASS [11]. AASS was powered by use of a typical voltage-fed full bridge series-resonant inverter. It employed a traditional zero-voltage switching (ZVS) full-bridge DC-AC inverter topology consisting of primary and secondary coils (L_1, L_2). The primary coil is located outside the body and generates an electromagnetic field. This time-varying field penetrates the skin and induces currents and voltages in the implanted secondary coil. A full wave rectifier and a charge-holding capacitor were used to convert the AC power to DC power. Next, a DC-DC voltage regulator stepped down this rectified voltage to a constant 5 V according to the requirements of AASS. For the sake of compensation on the primary side of a loosely coupled link, two tuning capacitors (C_1, C_2) were added to the primary and secondary circuits to enhance the power transfer capability.

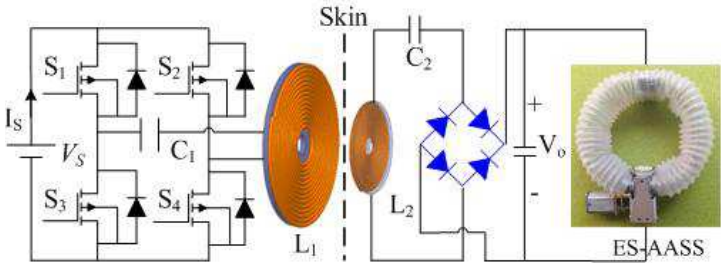

Figure 1. Schematic representation of a TETS consisting two planar spiral Litz-wire coils applied in AASS.

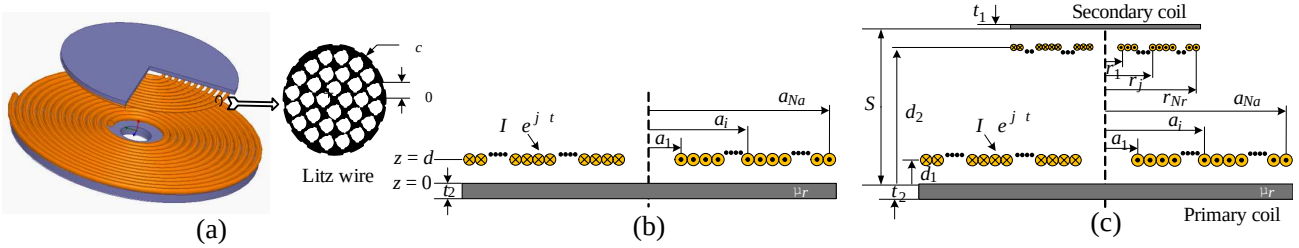

Figure 2. Planar Litz-wire coils with ferrite substrates. (a) Basic structure of coil pair. (b) Dimension description of single coil with ferrite substrate. (c) Dimension description of coil pair sandwiched with ferrite substrates.

2.2. Analytical Model of Coil

Figure 2 depicts the basic structure of the analyzed coil. In Figure 2(c), the primary and secondary coils have N_t and N_a Litz-wire concentric turns, with radii a_i ($i = 1, 2, \ldots, N_a$) and b_j ($j = 1, 2, \ldots, N_r$),

respectively. In this approach, the coil is modeled as a set of circular filamentary currents, each of which drives a current of amplitude I_Φ at an angular frequency ω. The linear, homogeneous, and isotropic ferrite substrate is characterized by its conductivity σ, relative permeability μ_r, and thickness t. The azimuthal electrical field $E_{\varphi,i}$ generated by a ith-turn of the separate coil in Figure 2(b) placed at (a_i, d), at any position (r, z) (such as $0 < z < d$) is done by [12]

$$E_{\phi,i}(r,z) = -\frac{j\omega\mu_0 I_\phi a_i}{2} \times \int_0^\infty e^{-kd}\left[e^{kz} - \lambda(t)\, e^{-kz}\right] J_1(kr)\, J_1(ka_i)\, dk \tag{1}$$

J_1 is the Bessel function of the first kind and order 1, and k is the integration variable. The parameter $\lambda(t)$ depends on material properties and is defined as

$$\lambda(t) = \phi(k)\, \frac{1 - e^{-2\eta t}}{1 - \phi(k)^2\, e^{-2\eta t}} \tag{2}$$

$$\phi(k) = (\mu_r - \eta/k) / (\mu_r + \eta/k) \tag{3}$$

$$\eta = \sqrt{k^2 + j\omega\mu_r\mu_0\sigma} \tag{4}$$

In the linear problem, the total electrical field can be computed applying the superposition principle as follows:

$$E_\phi(r,z) = \sum_{i=1}^{N_t} E_{\phi,i}(r,z) \tag{5}$$

The total induced voltage at the winding position $z = d$ is the sum of the voltage induced at each turn which can be calculated by integrating the $E_\Phi(r,z)$ along the winding length as follows:

$$V = -\sum_{j=1}^{N_t}\sum_{i=1}^{N_t}\int_0^{2\pi} E_{\phi,i}(r = a_j, z = d)\, a_j d\phi = -\sum_{j=1}^{N_t}\sum_{i=1}^{N_t} 2\pi a_j E_{\phi,i}(r = a_j, z = d) \tag{6}$$

therefore, the equivalent impedance is

$$Z = R_s + j\omega(L_0 + \Delta L) = \frac{V}{I_\Phi} \tag{7}$$

where R_S represents the losses due to the eddy currents in the substrate, L_0 the coreless inductance that will exist in the absence of the substrate, and ΔL the additional inductance due to the presence of the substrate.

$$\Delta L = \mu_0\pi \int_0^\infty \lambda_{real}(t) e^{-2kd} T(k) dk \tag{8}$$

The geometric function $T(k)$ in (11) is defined as

$$T(k) = \sum_{i=1}^{N_t} a_i^2 J_1^2(ka_i) + 2\sum_{i=1}^{N_t}\sum_{j>i}^{N_t} a_i a_j J_1(ka_i)\, J_1(ka_j) \tag{9}$$

where $\lambda_{real}(t)$ is the real part of the parameter $\lambda(t)$ defined in (7).

From [13], for condition $R/a \ll 1$, the self-inductance of a coil in air with a single-loop radius a and a wire radius R can be approximated as

$$L(a,R) = \mu_0 a\,(\ln(8a/R) - 2) \tag{10}$$

In addition, for perfectly aligned loops, the mutual inductance of the two parallel single-turn air-cored coils with loop radii of a and b can be expressed by using Equation (14), where d is the relative axial separation.

$$M_0(a,b,d) = \mu_0\sqrt{ab}\left[\left(\frac{2}{k} - k\right) K(k) - \frac{2}{k} E(k)\right] \tag{11}$$

where $K(k)$ and $E(k)$ are the complete elliptic integrals of the first and second kind respectively, and parameter k is defined in [13]. Thus, the self inductance L_0 of the coil in air composed of N_t concentric circular loops is the following

$$L_0 = \sum_{i=1}^{N_t} L\left(a_{1i}, R\right) + \sum_{i=1}^{N_t}\sum_{j=1}^{N_t} M_0\left(a_{1i}, a_{1j}, d=0\right)\left(1-\delta_{ij}\right) \tag{12}$$

From [14], the contribution of the ferrite substrates to the mutual inductance ΔM, shown in Figure 2(c), is given by the following expression

$$\Delta M = \mu_0 \pi \sum_{i=1}^{N_a}\sum_{j=1}^{N_r} a_i r_j \int_0^{\infty} J_1\left(kr_j\right) J_1\left(ka_i\right) \cdot \text{real}\left[f\left(\lambda\right) + g\left(\lambda\right)\right] dk \tag{13}$$

where

$$f\left(\lambda\right) = \frac{\lambda\left(t_1\right) e^{-k(d_1+d_2)} + \lambda\left(t_2\right) e^{-k\left(d_1'+d_2'\right)}}{1-\lambda\left(t_1\right)\lambda\left(t_2\right) e^{-2ks}} \tag{14}$$

$$g\left(\lambda\right) = \frac{2\lambda\left(t_1\right)\lambda\left(t_2\right) e^{-2ks}\cosh\left[k\left(d_2-d_1\right)\right]}{1-\lambda\left(t_1\right)\lambda\left(t_2\right) e^{-2ks}} \tag{15}$$

$$d_1' = S - d_1, \quad d_2' = S - d_2 \tag{16}$$

Considering Equations (14) and (16), the overall mutual inductance M can be obtained by adding the mutual inductance of the coil pair in the air and a contribution of the substrates ΔM.

$$M = \sum_{i=1}^{N_a}\sum_{j=1}^{N_r} M_0\left(a_i, r_j, d\right) + \Delta M \tag{17}$$

Therefore, an equation relating the self inductance and mutual inductance M to the coupling coefficient k is

$$k = M/\sqrt{L_P L_S} \tag{18}$$

2.3. FEA Simulated Model

In order to verify the validity of analytical expression related to the self inductance L and mutual inductance M, we adopted FEA with Maxwell V16.0. L and M as fundamental electrical engineering parameters for coil can be computed by applying the Bio-Savart law, Neumann's formula or other alternate methods [15, 16]. The results of the numerical solution deduced in [17] for the mutual inductance of two coaxial circular coils with rectangular cross section are in excellent agreement with that of the filament method [18]. Thus, in order to reduce the complexity of the model and save simulation time, two coaxial cylinder coils with rectangular cross section were adopted in FEA. Figure 3(a) illustrates the mesh created for the coil pair. The yellow components of the coils represent the copper windings with a conductivity of 5.8×10^7 S/m. The actual primary coil in the TETS had N_{t1} turns of Litz wire made with 400 strands of American-wire-gauge (AWG) 44 corresponding to a wire diameter of 1.7 mm; the secondary coil had N_{t2} turns of Litz wire made with 50 strands of AWG 44 corresponding to a wire diameter of 0.6 mm. The detailed design constraints were listed in Table 1. Thus, from the Maxwell software, the coil was modeled as a cylinder with an outer radius of r_o, inner radius of r_i, and a thickness of Φc, which was approximately equal to the diameter of the actual Litz wire. The primary and secondary ferrite substrates were also modeled according to the actual dimensions and properties.

Figure 3(b) illustrates the magnetic field density cross section contours around a primary and a secondary coil (P3S3 shown in Table 3) at an axial separation of 15 mm. The magnetic field in a sandwich structure is at its highest on the center facing the primary and slightly drops off on the face far away from the center. The overall magnetic field was evenly distributed in a large range through the internal radius to the external radius, and it greatly reduced the electric magnetic field above and below the secondary and primary windings.

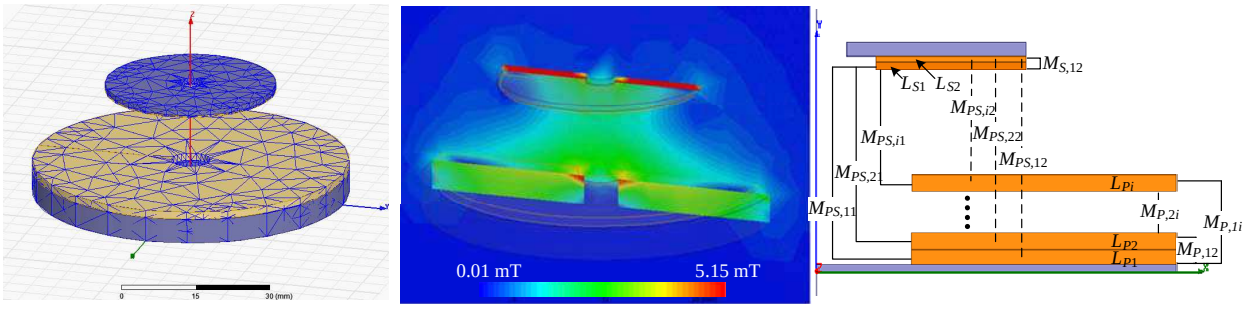

(a) (b) (c)

Figure 3. (a) 3-D Mesh of coil pair created in Maxwell software axially aligned. (b) Magnetic field distribution for an axial separation of 15 mm in a sandwich structure design. (c) Cross section of the 3-D simulation model.

Table 1. Design constraints imposed by application.

Parameters	P	S	Notes
$N_{l\max}$	5	2	Maximum number of layers
Φ_0 (mm)	0.05	0.05	Diameter of strand
N_S	400	50	Number of strands
Φ_c (mm)	1.7	0.6	wire diameter
$N_{t\max}$	16	25	Maximum number of turns
$r_{i\min}$ (mm)	2.8	2.5	Minimal coil inner radius
r_o (mm)	30	17.5	Coil external radius
D (mm)	10∼25		Coils relative distance (mm)

In order to investigate coupling effects caused by the coil number of layers, N_l, a 2-D simulation model with a rectangular cross-section (Figure 3(c)) was constructed to reduce the number of elements, and hence simulation time. Increasing the spread of the coil involves widening the cross-section. It was possible to operate with primary magnetic flux density (B) and field intensity (H) around the structures by the use of vector algebra and calculus operations through field calculator of the Maxwell program [19]. The self and mutual inductance of the separate coils (L_{Pi}, L_{Sj}, $M_{P,ij}$, $M_{S,ij}$ and $M_{PS,ij}$ shown in Figure 3(c)) can also be solved by the energy storage which is determined by the magnetic flux density and field intensity in the solution space. The overall self inductance and mutual inductance of this system can also be defined as follows

$$L = \sum_{i=1}^{N_l} L_i + \sum_{i=1}^{N_l}\sum_{j=1}^{N_l} M_{ij}\left(1-\delta_{ij}\right) \tag{19}$$

$$M = \sum_{i=1}^{N_{lP}}\sum_{j=1}^{N_{lS}} M_{PS,ij} \tag{20}$$

where N_{Lp} and N_{lS} are the primary and secondary number of layer, respectively.

3. OPTIMIZATION DESIGN

3.1. Design Constraints

The optimization approach employed as mentioned above is to use the analytical models and FEA to examine the combined effect of specific variables on k. According to step-by-step design procedure, a

set of design constrains as shown in Table 1 were utilized as a starting point to determine the optimal geometries and substrate properties of the coil pair in order to maximize the k. The design parameters that could be optimized included the number of turns N_t, number of layers N_l, substrate relative permeability μ_r, and substrate thickness t. Matlab-software producing 3D curves could demonstrate the changes in k when geometric parameters and substrate properties changed over a specific range.

3.2. Investigating Coupling Effects Due to N_t

The secondary μ_r and t, and primary μ_r and t with initial values ($\mu_r = 2000$, $t_1 = 0.5\,\text{mm}$, and $t_2 = 1\,\text{mm}$) were set before we started the optimization process for the N_{t1} and N_{t2} in consideration of the fact that these initial values might not be optimal. The maximum number of turns in a coil was defined in Table 1. Through plugging the initial values in (11), (15), (20) and (21), we found the k while sweeping N_{t1} and N_{t2} to be in a wide range around their initial values as shown in Figures 4(a) and (b) at a separation of coil pair of 10 mm and 20 mm, respectively. Figures 4(a) and (b) show that there was an optimal saturation value for N_{t2} beyond which there was no significant benefit to maximize the k as for every value of N_{t1}. As N_{t1} increased, k also increased; the best choice for N_{t1} was 14, and k almost flattened ($k = 0.358$) for $N_{t2} > 11$ with a separation distance of 10 mm. When the separation distance was changed to 25 mm, k almost reached at maximum value ($k = 0.121$) for $N_{t1} = 11$ and $N_{t2} = 10$. This indicated that the larger N_{t2} values were not better for improving the k at a fixed distance D. Therefore, we set $N_{t1} = 13$ and $N_{t2} = 11$ for the next optimization step.

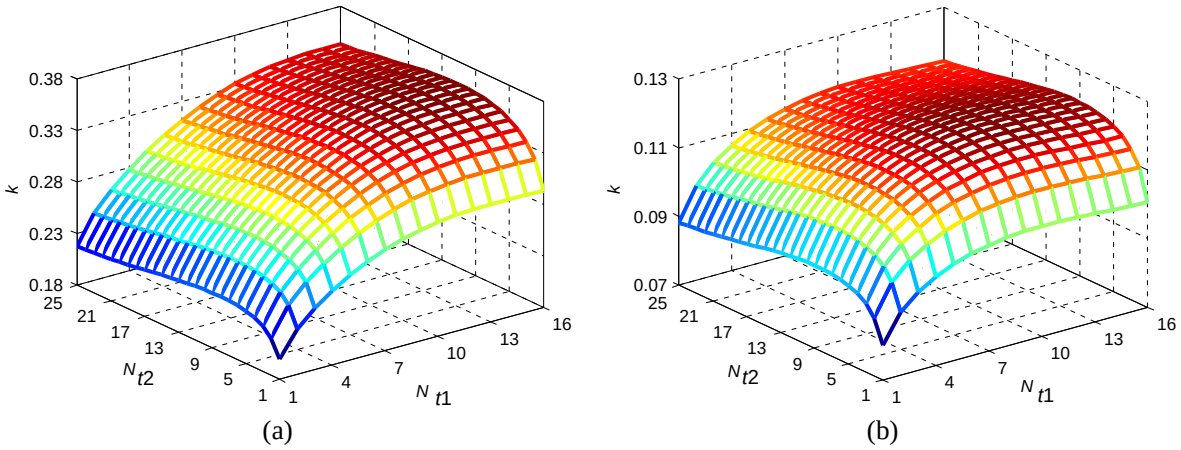

Figure 4. Optimizing the N_{t1} and N_{t2}. (a) $D = 10\,\text{mm}$. (b) $D = 25\,\text{mm}$.

3.3. Improving Coupling by Adding Ferrite

The effects of the ferrite disk as a part of the coil pair on magnetic field distributions in the vicinity of a TETS was first investigated, and the simulations for the coil structures presented in Figure 3(a) were performed using FEA. Careful examination of the magnetic field distribution is shown in Figure 5. To visualize the differences in the magnetic flux density distribution more clearly, the maximum limits of the color maps in Figure 5 were defined as 5200 μT. Figure 5(a) reveals that the magnetic flux density was strong near the coils without ferrite disks and significantly smaller than the case shown in Figure 5(b). Looking at Figure 5(b), there were clear differences in the magnetic field distributions. The magnetic flux density directly above and below the secondary and primary coils was significantly lower due to guiding and shielding effects on the magnetic field provided by the ferrite and the magnetic field generated by the coils with ferrite disks was strong and uniform in a larger range.

In this step, we studied the enhancement effect of the ferrite substrate on k. The parameter $\lambda(t)$, which depends on material properties defined in (4), contains four variables about the substrate of interest, i.e., t, μ_r, σ, and f, all of which positively affected the L and M by the magnetic field according to (11) and (16). Figure 6 shows k against t and μ_r of the ferrite substrates normalized by k_0

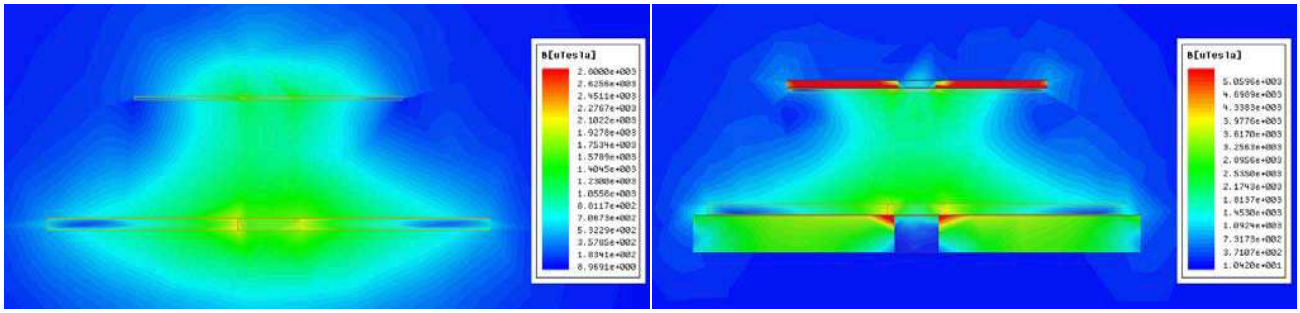

(a) (b)

Figure 5. Magnetic flux density distributions on XZ plane simulated under the condition of constant current excitation. (a) Both coils without ferrite substrate. (b) Both of coils with ferrite substrate.

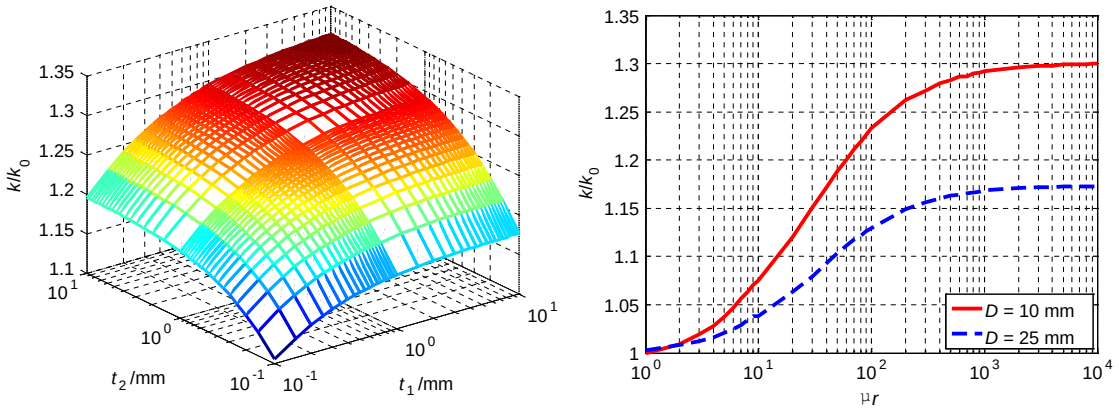

(a) (b)

Figure 6. Optimizing the μ_r and t of the ferrite substrate. (a) $D = 10\,\text{mm}$, k versus t_1 and t_2 with $\mu_r = 2000$. (b) The relationship between μ_r and k with $t_1 = 0.5\,\text{mm}$ and $t_2 = 1\,\text{mm}$.

which represents the coupling coefficient between the two coils in air without substrates ($k_0 = 0.279$ for $D = 10\,\text{mm}$, $k_0 = 0.092$ for $D = 25\,\text{mm}$). It was clear that an increase of either of the two variables was not continuously beneficial to the k. There were optimal values for u_r and t that maximized k. k was mostly benefited by an increase in u_r rather than by an increase in the thickness. The thicknesses of the primary and secondary coils were selected to be 0.5 mm and 1 mm, respectively in order to account for the size constrains and available materials. Figure 6(b) shows the calculated k as a function of u_r when the coil pair has 10 mm and 25 mm separations. It can be noted that the enhancement effect of the substrate was directly proportional to u_r; however, the contribution to k reached a saturation point at 0.361 for $u_r > 2000$ at 10 mm, and 0.124 for $u_r > 2000$ at 25 mm, respectively.

3.4. Relating Coupling Effects to Number of Layer

After optimizing N_t, t and μ_r, an attempt was made to investigate the relating coupling effect on number of layer N_l associated with the optimized parameters, which was characterized by $N_{t1} = 13$ ($r_{o1} = 7.9\,\text{mm}$), $N_{t2} = 11$ ($r_{o1} = 10.9\,\text{mm}$), $t_1 = 0.5\,\text{mm}$, $t_2 = 1\,\text{mm}$ and $\mu_r = 2000$. Here, the maximums N_l of primary and secondary coils were set at 5 and 2. Figures 7(a) and 8(b) show the effect of changing N_l on k when the two coils have a separation of 10 mm and 25 mm, respectively. For $D = 10\,\text{mm}$, as seen in Figure 7(a), k decreases as N_{l1} increases for every value of N_{l2}, and the value of k is slightly higher for $N_{l2} = 1$ than that for $N_{l2} = 2$ over the whole range of N_{l1}. The value of k reaches its maximum of 0.361 when $N_{l1} = 1$ and $N_{l2} = 1$. The whole changing trend of the relationship between the k and N_l for $D = 25\,\text{mm}$ conforms that of the condition for $D = 10\,\text{mm}$. Based on the

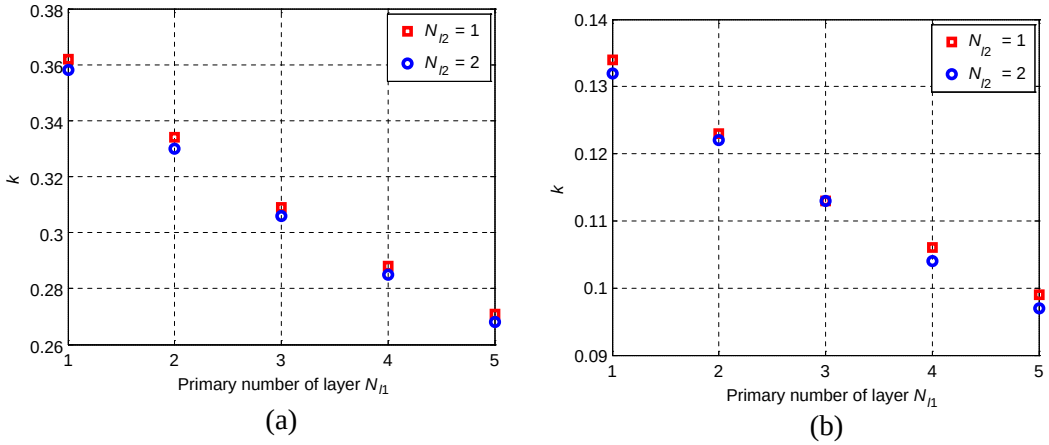

Figure 7. Optimizing the N_{l1} and N_{l2}. (a) $D = 10\,\text{mm}$. (b) $D = 25\,\text{mm}$.

above analysis, the final optimized values of the design example after step-by-step optimization can be set at $N_{t1} = 13$, $N_{t2} = 11$, $t_1 = 0.5\,\text{mm}$, $t_2 = 1\,\text{mm}$, $\mu_r = 2000$, $N_{l1} = 1$ and $N_{l2} = 1$, which yielded $k = 0.361$ for $D = 10\,\text{mm}$ and $k = 0.124$ for $D = 25\,\text{mm}$.

4. EXPERIMENTAL VERIFICATION

4.1. Experimental Setup

To evaluate the validity of the formula of determining the self- and mutual-inductance and the optimization methods presented in the previous sections, variable prototypes were fabricated with Litz wire as practical examples. The geometric and characteristic parameters of these coil pairs are shown in Table 2. Although these coils were not exactly the same as those with the theoretically optimal values found in Section 3, they validated the accuracy of our analytical models and simulation, and, by extension, the proposed optimization method. It should be noted that the ferrite material is brittle, especially when it has been fabricated into thin plates. In this paper, three kinds of available ferrite plates with a thicknesses of 0.5 mm, 1 mm and 5 mm were used. P0S0 represents the air-cored structure link, and the other represents the structure link with different values of N_t, N_l, t and μ_r described in Section 3.

Table 2. Specifications of the coil pairs used in experiments.

Parameter	Coil pair									
	P0	**S0**	**P1**	**S1**	**P2**	**S2**	**P3**	**S3**	**P4**	**S4**
N_t	16	18	16	18	13	11	13	11	13	11
l	1	1	1	1	1	1	1	1	2	2
r_{in} (mm)	2.8	6.7	2.8	6.7	7.9	10.9	7.9	10.9	7.9	10.9
r_{out} (mm)	30	17.5	30	17.5	30	17.5	30	17.5	30	17.5
t (mm)	-	-	0.5	1	0.5	1	5	1	5	1
μ_r	-	-	2000	2000	2000	2000	2000	2000	2000	2000

The practical self-inductance values were determined by measuring the coils in practice with a HIOKI 3532-50 impedance analyzer with an HP 16047A test fixture to achieve a higher accuracy in minimizing residual parameters and contact resistances. Figure 8(a) shows the practical measurement setup to measure the mutual inductance between the two coils. The primary coil was fixed at an upholder, and the secondary coil was mounted on a four-dimensional-coordinate moving workbench.

The relative position between the coil pair could be randomly adjusted. The axial distance between the coil pair would be approximately equal to the thickness of the patient's skin, fatty tissue, and muscle, and it was nominally between 10 to 25 mm [20]. Figure 8(b) shows an equivalent circuit for measuring the mutual inductance between coils, and R represents the equivalent series resistance (ESR) of coil. The primary coil was excited with an AC voltage V_i produced by a signal generator, and the secondary side voltage V_o was the open circuit voltage. The induced open voltage (V_o) at the secondary coil was measured by the use of oscilloscope, and the mutual inductance M was determined with the following formula:

$$M = L_1 V_o / V_i \tag{21}$$

4.2. Mutual Inductances between Coils

To analyze the enhancement effect of ferrite substrate on mutual inductance M numerically, 3-D FEA simulations for P0S0 and P1S1 were done in Maxwell v.16; to predict the M analytically, some analytical models were employed using the aforementioned parameters shown in Tables 1 and 2. The M curves as functions of axial separation for case P0S0 (air-cored structure) and case P1S1 (sandwiched structure) are plotted in Figure 9(a). Equation (11) was used for analytical prediction for M in case P0S0. To calculate the enhancement mutual inductance ΔM due to the contribution of the substrate, Equations (13) and (17) were employed in this model. The measured enhancement mutual inductance (ΔM

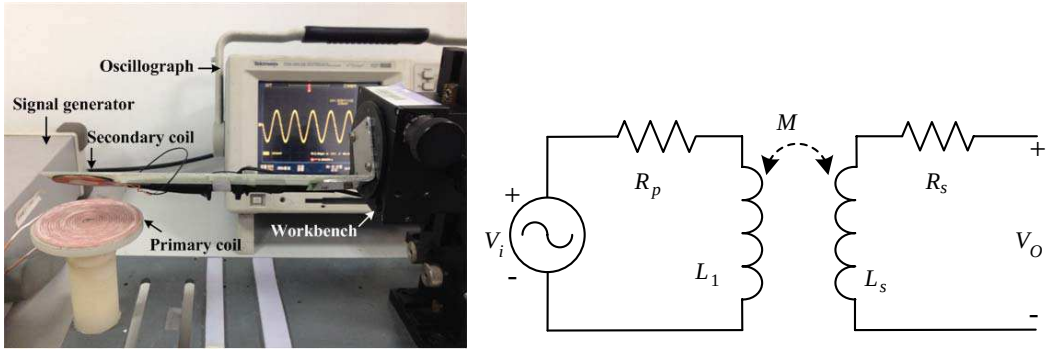

Figure 8. (a) Experimental setup: test coils and measurement system. (b) Equivalent circuit to measure mutual inductance.

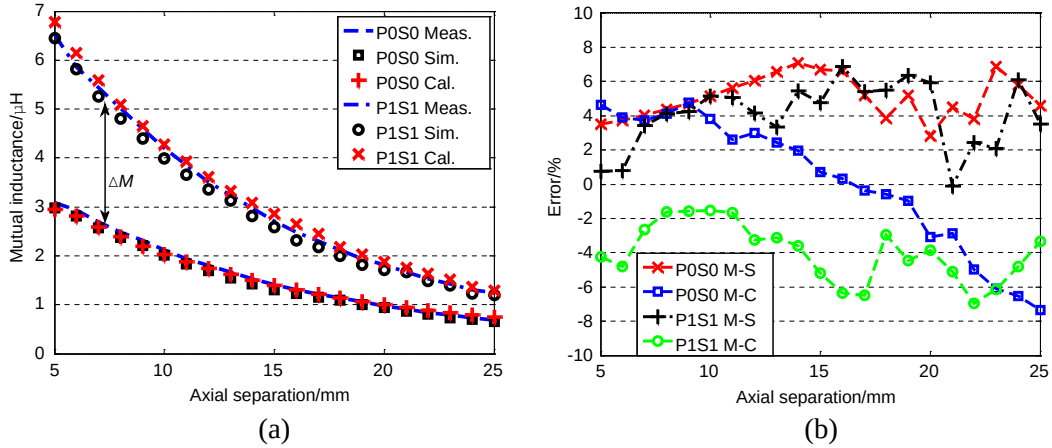

Figure 9. Measured, simulated and calculated mutual inductance M of four cases in a primary substrate structure: (a) comparison M of case 1 and case 5; (b) comparison M of case 3 and case 7.

measured) can be calculated by subtracting the measured results of case P1S1 from those of case P0S0. The simulated enhancement mutual inductance (ΔM simulated) can be obtained in the same way. The agreement among the measured, calculated, and simulated results was very good in all cases. Models Equations (11) and (17) can easily predict M and ΔM, respectively. These results in Figure 9(a) indicate that the mutual inductance between the primary and secondary coils can be enhanced when ferrite substrate is used and will be dropped with the increase of axial distance. The comparison among the measured, calculated, and simulated results in Figure 9(b) shows that the error between the calculated and measured results for case P0S0 is limited to 7.3%. The simulated results were also compared with the measured ones, and the error was limited to 6.4%. The maximum error among the measured, calculated, and simulated M for P1S1 was less than 6.8%.

4.3. Coupling Coefficients of Coils

Figure 10 illustrates the measured, calculated, and simulated results related to the coupling coefficient when the axial separation is increased from 5 mm to 25 mm for the five kinds of coil pairs. As expected, the coupling coefficient decreases as the separation increases under the condition of axially aligned coils. All three methods produced consistent results. Results from Figure 10(a) shows that significant enhancement of coupling coefficient can be achieved by using ferrite substrate. Figure 10(b) shows that the same order of magnitude on coupling strength can be obtained from the coil pair with a small number of turns placed near the edge of the winding area over the entire structure, and an explanation for this observation could be the magnetic flux distribution associated with the innermost radius of the winding [21]. The magnetic field intensity of the winding with a smaller inner radius was the

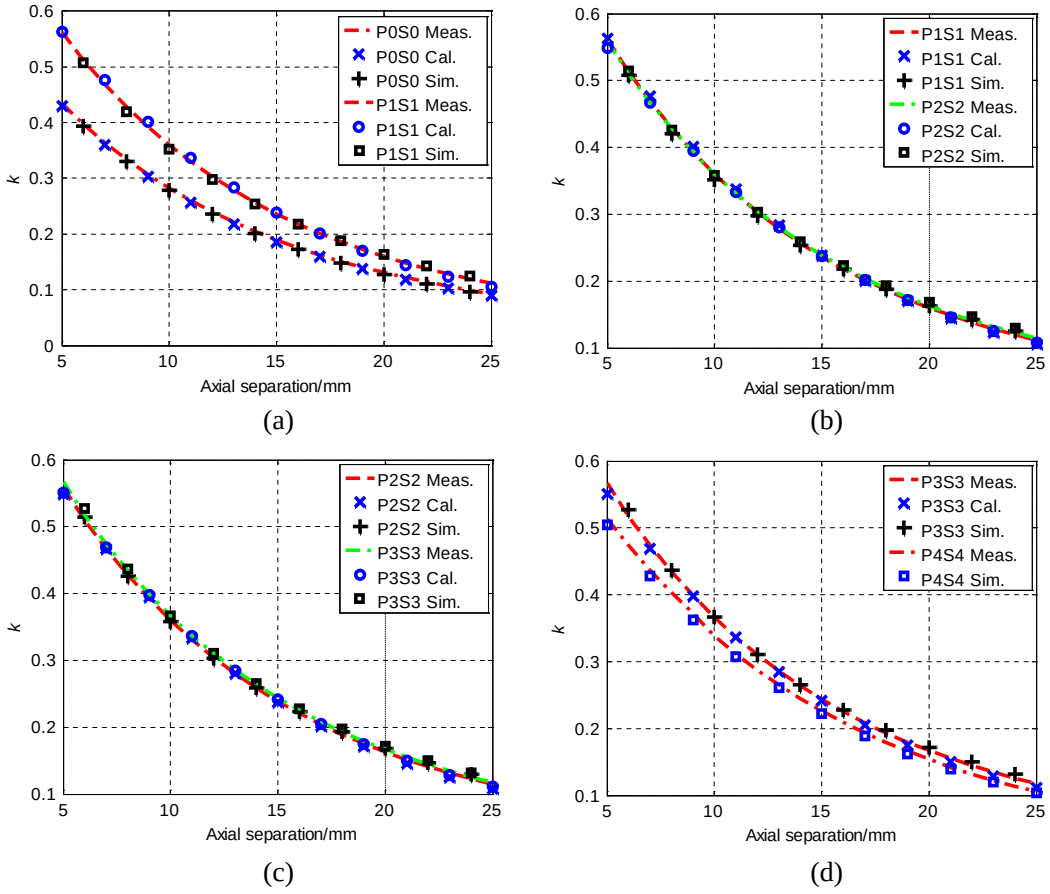

Figure 10. Measured, simulated and calculated coupling coefficient k of different coil pairs shown in Table 2.

highest in the central region and dropped quickly from the center to the periphery of the spiral winding; by contrast, the magnetic field distribution of the winding with a relatively large innermost radius decreased evenly and slowly from the periphery to the center. This is an important observation in the planar spiral winding design. In our design, the outermost radii of the primary and secondary coil were fixed, which led to a type of coil pair with an optimal innermost radius to obtain the best coupling coefficient. Figures 10(c) and 11(d) show the effect of changing the two design parameters of t and N_l on the value of k, respectively. It is found that the results shown in these figures are consistent with the theoretical analysis of the optimization design described in Section 3.

5. CONCLUSION

The proposed optimization design of Litz-wire coil pair with ferrite substrate has shown an excellent performance in TETS. A series of formulas of self- and mutual-inductance for two coaxial Litz-wire coils sandwiched between two ferrite substrates have been established. These formulas were based on the physical dimensions (N_t and N_l) of the coil and with electromagnetic properties (t and μ_r) of the ferrite substrate considered. A step-by-step procedure was devised to optimize the parameters of N_t, N_l, t, and μ_r for such coil pair to maximize k. Furthermore, several coil pairs were also fabricated and tested to validate the design procedure. All calculated, simulated and measured results were in good agreement within the design constrains, which demonstrated the validity of the models and proposed optimal design.

REFERENCES

1. Okamoto, E., Y. Yamamoto, Y. Akasaka, T. Motomura, Y. Mitamura, and Y. Nosé, "A new transcutaneous energy transmission system with hybrid energy coils for driving an implantable biventricular assist device," *Artif. Organs*, Vol. 33, No. 8, 622–626, 2009.
2. Ruthmann, O., S. Richter, G. Seifert, et al., "The first teleautomatic low-voltage prosthesis with multiple therapeutic applications: A new version of the German artificial sphincter system," *Artif. Organs*, Vol. 34, No. 8, 635–641, 2010.
3. Ke, L., G. Z. Yan, H. Liu, et al., "A novel artificial anal sphincter system in an in Vitro and in Vivo experiment," *Int. J. Artif. Organs*, Vol. 37, No. 3, 253–263, 2014.
4. Luo, Y. H. L. and L. D. Cruz, "A review and update on the current status of retinal prosthesis (bionic eye)," *Br. Med. Bull.*, Vol. 109, No. 1, 31–44, 2014.
5. Cho, S. H., N. Xue, L. Cailler, et al., "A SU-8-based fully integrated biocompatible inductively powered wireless neurostimulator," *J. Microelectromech S.*, Vol. 22, No. 2, 170–176, 2013.
6. Xue, N., S. H. Cho, S. P. Chang, and J. B. Lee, "Systematic analysis and experiment of inductive coupling and induced voltage for inductively coupled wireless implantable neurostimulator application," *J. Micromech. Microeng.*, Vol. 22, No. 7, 075008-1–075008-10, 2012.
7. Laskovski, A. N., M. R. Yuce, and T. Dissanayake, "Stacked spirals for biosensor telemetry," *IEEE Sensors J.*, Vol. 11, No. 6, 1484–1490, 2011.
8. Qusba, A., A. K. RamRakhyani, J. H. So, G. J. Hayes, M. D. Dickey, and G. Lazzi, "On the design of microfluidic implant coil for flexible telemetry system," *IEEE Sensors J.*, Vol. 14, No. 4, 1074–1080, 2014.
9. Valtchev, S., B. Borges, K. Brandisky, and J. B. Klaassens, "Resonant contactless energy transfer with improved efficiency," *IEEE Trans. Power Electron.*, Vol. 24, No. 3, 685–699, 2009.
10. Budhia, M., G. A. Covic, and J. T. Boys, "Design and optimization of circular magnetic structures for lumped inductive power transfer systems," *IEEE Trans. Power Electron.*, Vol. 26, No. 11, 3096–3108, 2011.
11. Ke, L., G. Z. Yan, and S. Yan, "Feedback control of TET system with variable coupling coefficients for a novel artificial anal sphincter," *J. Med. Eng. Technol.*, Vol. 38, No. 2, 90–99, 2014.
12. Hurley, W. G. and M. C. Duffy, "Calculation of self and mutual impedances in planar sandwich inductors," *IEEE Trans. Magn.*, Vol. 33, No. 3, 2282–2289, 1997.

13. Zierhofer, C. M. and E. S. Hochmair, "Geometric approach for coupling enhancement of magnetically coupled coils," *IEEE Trans. Biomed. Eng.*, Vol. 43, No. 7, 708–714, 1996.
14. Ke, L., G. Z. Yan, S. Yan, Z. W. Wang, and D. S. Liu, "Coupling analysis of TET coils with planar sandwich structure for a novel artificial anal sphincter," *Journal of Zhejiang University — Science C*, 2014.
15. Zhong, G. and C. K. Koh, "Exact closed form formula for partial mutual inductance of on-chip interconnects," *Proc. 2002 IEEE Int. Conf. Computer Design: VLSI in Computers and Processors, ICCD*, 428–433, 2012.
16. Babic, S., S. J. Salon, and C. Akyel, "The mutual inductance of two thin coaxial disk coils in air," *IEEE Trans. Magn.*, Vol. 40, No. 2, 822–825, 2004.
17. Babic, S. I. and C. Akyel, "New analytic-numerical solutions for the mutual inductance of two coaxial circular coils with rectangular cross section in air," *IEEE Trans. Magn.*, Vol. 42, No. 6, 1661–1669, 2006.
18. Kim, K. B., E. Levi, Z. Zabar, and L. Birenbaum, "Mutual inductance of noncoaxial circular coils with constant current density," *IEEE Trans. Magn.*, Vol. 33, No. 5, 3916–3921, 1997.
19. ANSYS, Inc., "Ansoft Maxwell 3D field simulator v11 user's guide," Ansoft Corporation, Rev. 2.0, 2006.
20. Dissanayake, T. D., P. A. Hu, S. Malpas, et al., "Experimental study of a TET system for implantable biomedical devices," *IEEE Trans. Biomed. Circuits Syst.*, Vol. 3, No. 6, 370–378, 2009.
21. Liu, X. and S. Y. Hui, "Optimal design of a hybrid winding structure for planar contactless battery charging platform," *IEEE Trans. Power Electron.*, Vol. 23, No. 1, 455–463, 2008.